
Deep Active Learning with Noise Stability

Xingjian Li^{1,2,*}, Pengkun Yang^{3,*}, Tianyang Wang⁴, Xueying Zhan¹,
Min Xu⁵, Dejing Dou¹, Chengzhong Xu²

¹Big Data Lab, Baidu Research

²State Key Lab of IOTSC, Department of Computer Science, University of Macau

³Center for Statistical Science, Tsinghua University

⁴Austin Peay State University

⁵Carnegie Mellon University

Abstract

Uncertainty estimation for unlabeled data is crucial to active learning. With a deep neural network employed as the backbone model, the data selection process is highly challenging due to the potential over-confidence of the model inference. Existing methods resort to special learning fashions (e.g. adversarial) or auxiliary models to address this challenge. This tends to result in complex and inefficient pipelines, which would render the methods impractical. In this work, we propose a novel algorithm that leverages noise stability to estimate data uncertainty in a Single-Training Multi-Inference fashion. The key idea is to measure the output derivation from the original observation when the model parameters are randomly perturbed by noise. We provide theoretical analyses by leveraging the small Gaussian noise theory and demonstrate that our method favors a subset with large and diverse gradients. Despite its simplicity, our method outperforms the state-of-the-art active learning baselines in various tasks, including computer vision, natural language processing, and structural data analysis.

1 Introduction

The success of training a deep neural network highly depends on a huge amount of labeled data. However, much data is unlabeled in the era of big data, and data annotation cost could be extremely high, such as in medical area [1, 2]. Due to limited annotation budget, it might be more feasible to annotate a portion of the given data. Then a question can be naturally raised: which data is deserved for being annotated?

Active learning was proposed to solve this question. One of the main ideas, namely *uncertainty-based* method, aims to select the most uncertain/informative data from an unlabeled pool for annotation. The newly annotated data is then used to train a task model. Note that uncertainty estimation with deep neural networks (DNNs) remains challenging, due to the potential over-confidence of deep models [3]. That is, the primitive softmax output* (as a score) does not necessarily reflect a reliable uncertainty or confidence for the prediction. Several methods have been proposed to address this challenge. For example, deep Bayesian methods [4] suggest to estimate the entropy (or other indicators such as mutual information) with the posterior predictive probability over the model parameters. Gal and Ghahramani [4] implement a Single-Training Multi-Inference algorithm by aggregating multiple confidences sampled by Monte Carlo dropout. Another typical approach is query-by-committee (QBC) [5, 1], which requires training multiple auxiliary models to form a committee. Besides, many other efforts suggest to use specially designed auxiliary models or training fashions, such as variational auto-encoder [6], Graph Convolutional Network [7], and adversarial learning [8, 9].

*Equal contribution.

*Considering classification problems.

In this work, we study the problem of deep active learning from a different perspective, inspired by a relevant topic of *noise stability*, which, in terms of the output stability w.r.t. the input noise, is well studied in literature. For example, Bishop [10] proposes to train a model with perturbed input examples as a regularizer to improve the model performance. Arora et al. [11] show that, the stability of each layer’s computation towards input noise, injected at lower layers, acts as a good indicator of the generalization bounds for DNNs. An intuition behind these achievements is that, a model (or more exactly, its parameters) robust to perturbed input examples tends to easily recognize unobserved samples. For active learning, we give an analogous intuition by exchanging the role of the input and the model parameters. That is, a data example which is robust to the perturbed parameters, tends to be easily recognized by a future model. In other words, *data examples which are less robust to the parameter perturbation could be regarded as having higher uncertainty*.

Furthermore, the output deviation also reveals direction information, which facilitates a diverse subset selection from the unlabeled pool. Intuitively, when a randomly sampled perturbation is imposed on the entire network, some neurons (corresponding to some specific patterns) may be distorted more than others. If these patterns are not essential (e.g. not activated by the ReLU function) for an example, a small noise on the corresponding neurons will probably lead to a stable feature embedding. Otherwise, the examples, which are highly depending on these patterns, will induce larger deviations from the feature embedding, i.e. the elements relevant to these patterns will change remarkably. In this sense, *our data selection criterion also takes into account the stability w.r.t. different feature directions*, given a specific parameter noise.

In light of the aforementioned intuitions, we design a simple deep active learning algorithm by measuring the output deviation from the original observation, when imposing a small noise on the model parameters. The magnitude of the deviation acts as a metric of uncertainty, and the direction is utilized to constitute a diverse subset of selected unlabeled examples. We provide a theoretical analysis under the condition that the noise magnitude is small. By imposing standard multivariate Gaussian noise to the parameters, we prove that the induced deviation yields a sort of *projected gradient*. The expectation of the magnitude of this gradient is equivalent to the gradient norm w.r.t the model parameters, whereas the direction of this gradient serves as a proxy of the direction of the original gradient.

Our method is easy to implement and free of data-dependent designs or customized auxiliary models. Therefore, it can be exploited in classification, regression and more complex tasks such as semantic segmentation. It is also applicable to various data domains such as image, natural language and structural data. We evaluate our method on multiple tasks, including (1) image classification on MNIST [12], Cifar10 [13], SVHN [14], Cifar100 [13], and Caltech101 [15]; (2) regression on the Ames Housing dataset [16]; (3) semantic segmentation on Cityscapes [17]; and (4) natural language processing on MRPC [18]. We demonstrate that our method exceeds or is comparable to the state-of-the-art baselines on all these tasks.

The contributions of this work are summarized as follows.

1. We propose a novel deep active learning method, namely *NoiseStability*, to select unlabeled data for annotation. It is free of any auxiliary models or customized training fashions. We conduct extensive experiments on diverse tasks and data types to demonstrate the general applicability and superior performance of our method.
2. We prove that selecting unlabeled data w.r.t. noise stability is theoretically equivalent to selecting data according to randomly projected gradients. Conditioned on standard Gaussian noise, the induced feature deviation exhibits decent properties in both estimating uncertainty and ensuring diversity.

2 Deep Active Learning with Noise Stability

2.1 Problem Definition

Here we formulate the deep active learning problem. Given a pool of unlabeled data $\{X_U\}$, and a labeled pool $\{X_L, Y_L\}$ which is initially empty. Active learning aims to select a portion of data from $\{X_U\}$ depending on an annotation budget (e.g. select 2500 samples out of 50000 at a time). The selected data X_N is then annotated by human oracles (or equivalent), and added to the labeled pool. That is, $\{X_L, Y_L\} \leftarrow \{X_L, Y_L\} + \{X_N, Y_N\}$, where Y_N is the new annotation for X_N . The

Algorithm 1: Deep Active learning with noise stability.

Input : \mathcal{T} : random initialized task model, \mathcal{U} : unlabeled pool of training data, \mathcal{L} : labeled pool of training data, \mathcal{C} : number of cycles in active learning;
Output : θ, ϕ : Final learned parameters of \mathcal{T} ;

```
1 begin
2   for  $i \leftarrow 1$  to  $\mathcal{C}$  do
3     train  $\mathcal{T} = g \circ f$  with  $\mathcal{L}$ , obtaining the current parameters  $\theta, \phi$ ;
4     for  $k \leftarrow 1$  to  $K$  do
5       sample a random direction  $\mathbf{u}^{(k)}$  and get  $\Delta\theta^{(k)} = \zeta\|\theta\|_2\mathbf{u}^{(k)}$ ;
6       for every  $\mathbf{x}$  in  $\mathcal{U}$  do
7         for  $k \leftarrow 1$  to  $K$  do
8           calculate  $\Delta z(\mathbf{x})^{(k)} = f(\mathbf{x}; \theta + \Delta\theta^{(k)}) - f(\mathbf{x}; \theta)$ ;
9           get  $\widehat{\Delta z}(\mathbf{x})$  by concatenating all  $\Delta z(\mathbf{x})^{(k)}$  for  $k = 1, 2, \dots, K$ ;
10        compute  $N$  centers  $\{c_j\}_{j=1}^N$  w.r.t.  $\{\widehat{\Delta z}(\mathbf{x}) | \mathbf{x} \in \mathcal{U}\}$  by greedy k-center algorithm;
11        select samples whose indexes are  $\{c_j\}_{j=1}^N$  in  $\mathcal{U}$  as  $\{X_N\}$ , and obtain their labels  $\{Y_N\}$ ;
12        update  $\mathcal{L}$  with  $\mathcal{L} = \mathcal{L} \cup \{X_N, Y_N\}$ ;
13        update  $\mathcal{U}$  with  $\mathcal{U} = \mathcal{U} \setminus \{X_N\}$ ;
14   return  $\theta, \phi$ ;
```

unlabeled pool is then updated by removing the selected data: $\{X_U\} \leftarrow \{X_U\} - \{X_N\}$. The updated $\{X_L, Y_L\}$ is then used to train a task model composed of a feature extractor f followed by a task head g . f and g are parameterized by θ and ϕ , respectively. We use $f(\cdot; \theta)$ and $g(\cdot; \phi)$ to denote the corresponding feed-forward operations of f and g . Note that the feature extractor f is normally a deep neural network of which parameters $\theta \in \mathcal{R}^n$ are in high dimension. In contrast, the architecture of g is arguably shallow, e.g. a single fully connected layer for classification or regression problems.

2.2 Uncertainty Estimation with Noise Stability

We aim at investigating how intermediate representations change when a small perturbation is imposed on model parameters. Specifically, given x as an input, we consider the output of the feature extractor, i.e. $z = f(\mathbf{x}; \theta) \in \mathcal{R}^d$. Let $\Delta\theta \in \mathcal{R}^n$ denote the added noise (perturbation) and $\Delta\theta = \zeta\|\theta\|_2\mathbf{u}$, where ζ controls the relative magnitude of the noise and \mathbf{u} is a random direction with the unit length.[†] ζ should be relatively small (e.g. 10^{-3}) in order to avoid a catastrophic perturbation to the clean model. Then, for an unlabeled sample $\mathbf{x} \in X_U$, its feature deviation is

$$\Delta z(\mathbf{x}) = \frac{1}{\zeta\|\theta\|_2} (f(\mathbf{x}; \theta + \Delta\theta) - f(\mathbf{x}; \theta)). \quad (1)$$

For brevity, we assume z and Δz are both row vectors, and use $\Delta\theta^{(k)}$ to denote the k -th sampled parameter noise. We perform K samplings of $\Delta\theta$ and concatenate all the resulting feature deviations as

$$\widehat{\Delta z}(\mathbf{x}) = \sqrt{\frac{n}{K}} (\Delta z(\mathbf{x})^{(1)}, \Delta z(\mathbf{x})^{(2)}, \dots, \Delta z(\mathbf{x})^{(K)}), \quad (2)$$

where $\widehat{\Delta z}(\mathbf{x}) \in \mathcal{R}^{Kd}$ is the empirical result and each $\Delta z(\mathbf{x})^{(k)}$ corresponds to the feature deviation produced by the parameter noise $\Delta\theta^{(k)}$.

Here we adopt the empirical feature deviation $\widehat{\Delta z}(\mathbf{x})$ as the representation of each unlabeled example \mathbf{x} . The rationale lies in two aspects. Firstly, in active learning, we favor data with higher uncertainty w.r.t. the current learned model. Such data are usually hard examples that tend to be sensitive to small parameter perturbations. Therefore, the length of $\widehat{\Delta z}(\mathbf{x})$ can be used as a criterion for uncertainty estimation. Secondly, the direction of $\widehat{\Delta z}(\mathbf{x})$ implies potential characteristics of an example \mathbf{x} , that is, which learned feature components are sensitive (or not robust) to a parameter perturbation. Diverse currently non-robust features should be focused on, in order to learn more comprehensive knowledge.

[†]In practice, \mathbf{u} can be sampled from a standard multivariate Gaussian distribution and then normalized by its own L^2 -norm.

Due to its relevance to data diversity, the direction of $\widehat{\Delta z}(\mathbf{x})$ can be utilized to select a batch of samples, where the diversity of selected examples is also essential to a good performance [19, 20].

Considering both magnitude and direction, we use Gonzalez’s greedy implementation [21] of the k-center algorithm for diverse subset selection. As pointed out in BADGE [22], a diverse subset will naturally prefer examples with larger magnitudes as they tend to be far away from each other if measured in a Euclidean space. The pipeline of our method is summarized in Algorithm 1.

3 Theoretical Understandings

In this section, we present theoretical understandings of our method for deep active learning. Our main conclusions are summarized as follows.

- When the noise magnitude $\zeta\|\boldsymbol{\theta}\|$ is sufficiently small, for a given example \mathbf{x} , the expectation of $\|\widehat{\Delta z}(\mathbf{x})\|_2$ is the Frobenius norm of the Jacobian of f w.r.t. its parameters $\boldsymbol{\theta}$, when proper prerequisites are satisfied for \mathbf{u} .
- Considering the 1-d case $f : X \rightarrow \mathcal{R}$, the suggested $\widehat{\Delta z}(\mathbf{x})$ can be regarded as a projected gradient, which has a much lower dimension compared to the original gradient $\nabla_{\boldsymbol{\theta}} f$. With the projected gradient being employed, the spatial relationships (e.g. Euclidean distance and inner product) among examples remain the same as if the original gradient is being used, indicating $\widehat{\Delta z}(\mathbf{x})$ a reasonable proxy of the original gradient, when considering diversity.

3.1 Noise Stability as Jacobian Norm

Let $f(\mathbf{x}; \boldsymbol{\theta})$ be differentiable (w.r.t. $\boldsymbol{\theta}$) at $\boldsymbol{\theta} \in \mathcal{R}^n$ given \mathbf{x} as an input. When the imposed noise $\Delta\boldsymbol{\theta} = \zeta\|\boldsymbol{\theta}\|_2\mathbf{u}$ has a sufficiently small magnitude, i.e. in the limit as $\zeta \rightarrow 0$, we use the first-order Taylor expansion to represent the perturbed output $f(\mathbf{x}; \boldsymbol{\theta} + \Delta\boldsymbol{\theta})$ as

$$f(\mathbf{x}; \boldsymbol{\theta} + \Delta\boldsymbol{\theta}) = f(\mathbf{x}; \boldsymbol{\theta}) + \mathbf{J}_{\boldsymbol{\theta}}(\mathbf{x}; \boldsymbol{\theta})\Delta\boldsymbol{\theta} + o(\zeta\|\boldsymbol{\theta}\|_2), \quad (3)$$

where $\mathbf{J}_{\boldsymbol{\theta}}(\mathbf{x}; \boldsymbol{\theta})$ denotes the Jacobian matrix of f w.r.t the parameters $\boldsymbol{\theta}$ as $\mathbf{J}_{\boldsymbol{\theta}}(\mathbf{x}; \boldsymbol{\theta})_{(i,j)} = \partial f(\mathbf{x}; \boldsymbol{\theta})_{(i)} / \partial \boldsymbol{\theta}_{(j)}$. By applying the Taylor approximation, each block $\Delta z(\mathbf{x})^{(k)}$ can be formulated as

$$\Delta z(\mathbf{x})^{(k)} = \mathbf{J}_{\boldsymbol{\theta}}(\mathbf{x}; \boldsymbol{\theta})\mathbf{u}^{(k)} + o(1). \quad (4)$$

By omitting the higher order term $o(1)$, it results in the output deviation magnitude to be

$$\|\widehat{\Delta z}(\mathbf{x})\|_2^2 = \frac{n}{K} \sum_{k=1}^K \|\mathbf{J}_{\boldsymbol{\theta}}(\mathbf{x}; \boldsymbol{\theta})\mathbf{u}^{(k)}\|_2^2. \quad (5)$$

Conditioned on the elements of $\mathbf{u}^{(k)}$ are zero-mean and independent of each other, it can be derived that the expectation of the data selection metric (i.e. $\|\widehat{\Delta z}(\mathbf{x})\|_2$) is equivalent to the Frobenius norm of Jacobian as

$$\mathbb{E}_{\mathbf{u}} \|\widehat{\Delta z}(\mathbf{x})\|_2^2 = \|\mathbf{J}_{\boldsymbol{\theta}}(\mathbf{x}; \boldsymbol{\theta})\|_F^2. \quad (6)$$

We put a detailed proof of Eq (6) in Appendix A.1 using the Standard multivariate Gaussian distribution as a demonstration. In fact, Eq (6) is satisfied for any appropriate noise distributions with the aforementioned prerequisite of independence and zero mean. We also provide a quantified concentration inequality, showing that $\|\widehat{\Delta z}(\mathbf{x})\|_2^2$ can be close to the Jacobian norm with high probability in Appendix A.1.

3.2 Diversified Projected Gradients

Since $\widehat{\Delta z}(\mathbf{x})$ indicates which directions (i.e. elements of the final feature) of an example is more sensitive to a specific parameter perturbation, it can be employed to select diverse examples to constitute a subset. By applying the first order Taylor expansion, each $\widehat{\Delta z}(\mathbf{x})$ can be regarded as a *projected gradient* when the output of f is a scalar (here we ignore the Jacobian matrix for simplicity). That is, the original gradient $\nabla_{\boldsymbol{\theta}} f$ is transformed by random directions $\{\mathbf{u}^{(k)}\}_{k=1}^K$ to its projected format as shown in Eq (4).

The benefit of diverse gradients has been discussed in existing literature. For example, a recent work [23] theoretically shows that, performing SGD with diversified gradients within a mini-batch helps lower the variance of stochastic gradients. BADGE [22] selects diverse examples according to their last layer’s gradients rather than considering that of the entire model. Here we show that, leveraging the expectation of the projected gradients $\{\widehat{\Delta z}(\mathbf{x})|\mathbf{x} \in \mathcal{U}\}$ is equivalent to using $\{\nabla_{\theta} f(\mathbf{x}; \theta)|\mathbf{x} \in \mathcal{U}\}$. Specifically, given two examples \mathbf{x}_i and \mathbf{x}_j , the following two properties hold.

Property 1. *Equivalence of Euclidean distance.*

$$\mathbb{E}_{\mathbf{u}} \|\widehat{\Delta z}(\mathbf{x}_i) - \widehat{\Delta z}(\mathbf{x}_j)\|_2^2 = \|\nabla_{\theta} f(\mathbf{x}_i; \theta) - \nabla_{\theta} f(\mathbf{x}_j; \theta)\|_2^2. \quad (7)$$

Property 2. *Equivalence of inner product.*

$$\mathbb{E}_{\mathbf{u}} \langle \widehat{\Delta z}(\mathbf{x}_i), \widehat{\Delta z}(\mathbf{x}_j) \rangle = \langle \nabla_{\theta} f(\mathbf{x}_i; \theta), \nabla_{\theta} f(\mathbf{x}_j; \theta) \rangle. \quad (8)$$

We put a detailed proof of these properties in Appendix A.2. Similarly, we will also show that our estimated Euclidean distance and inner product are close to their respective expectations with high probability.

The above analyses lead to the following conclusion: subset selection with $\{\widehat{\Delta z}(\mathbf{x})|\mathbf{x} \in \mathcal{U}\}$ is approximately equivalent to that with $\{\nabla_{\theta} f(\mathbf{x}; \theta)|\mathbf{x} \in \mathcal{U}\}$, by using either distance-based (e.g. greedy-k-center) or similarity-based algorithms (e.g. k-DPP).

3.3 Connections to Related Methods

The Expectation Gradient Length (EGL) has been shown as an effective criterion for uncertainty measurement [24]. One practical issue is that, actual labels remain unknown in advance. A common solution is to marginalize over all possible labels [25, 22] or over top-k mostly possible labels [26]. However, these solutions are usually costly or even infeasible for some complex tasks. Another challenge is the extremely huge dimension of gradients (w.r.t. model parameters) when using gradient directions. A recent state-of-the-art method BADGE [22] addresses this challenge by only considering the last layer of DNNs.

Now we present a detailed comparison with BADGE. In a multiclass classification problem with softmax activations, given a loss function L , BADGE yields the i -th block of the gradient of an example \mathbf{x} as

$$\nabla_{\phi_i} L = (p_i - I(\hat{y} = i))f(\mathbf{x}; \theta), \quad (9)$$

where ϕ_i is the i -th row parameters of ϕ , and p_i is the probability for label i , thus $\hat{y} = \arg \max_i p_i$.

Though our method (based on noise stability) is highly relevant to gradients as shown in Eq (4), there are two essential differences with BADGE (as well as other related works).

- Noise stability avoids explicitly approximating gradients, and hence does not require assuming and marginalizing pseudo labels, which will result in expensive computations. Such an issue can be fatal in complex scenarios. For example, in semantic segmentation (or speech recognition), the number of label assumptions increases exponentially with increase in the number of pixels (or timesteps). Therefore, it is infeasible to gather the gradients w.r.t. all possible labels. Moreover, poor calibration of DNNs can be detrimental to the estimation of probabilistic predictions [27], i.e. p_i in Eq (9).
- In terms of final representations, noise stability resorts to *projected gradients* w.r.t. feature, while BADGE actually relies on *feature itself* and probabilistic predictions. In terms of uncertainty estimation, the gradient magnitude $\|\nabla_{\theta} f(\mathbf{x}; \theta)\|_2$ is a more meaningful indicator than the magnitude of $f(\mathbf{x}; \theta)$. Besides, in a regression problem, Eq (9) is meaningless due to the infeasibility of assuming a ground truth label and has to resort to the original feature only. In contrast, noise stability is still applicable, taking into account both uncertainty and diversity.

3.4 Implementation Tips

In practice, for a deep neural network we can compute the perturbation $\widehat{\Delta z}(\mathbf{x})$ w.r.t. the final deep feature. However, for a classification network, it is also feasible to employ the final predictive output

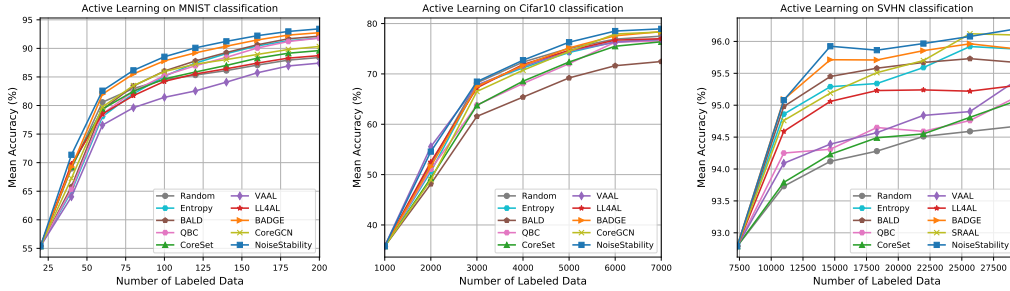


Figure 1: Classification performance due to the different active learning methods on MNIST (left), Cifar10 (middle) and SVHN (right).

to measure noise stability, since such an output can be regarded as a high-level semantic feature. Moreover, the predictive output usually compresses the primitive deep feature, thus resulting in a vector with a lower dimension. In applications with a large pool size and a high annotation budget, adopting the predictive output will naturally lead to an efficient implementation. Therefore, we suggest to compute the deviation on the predictive output for classification tasks, and on the final deep feature for other tasks such as regression and semantic segmentation.

4 Experimental Results

We compare our method with the state-of-the-art active learning baselines. Since Random selection is simple yet effective, we also include it as a baseline. We firstly validate our method on image classification tasks in Section 4.1. Then in Section 4.2, we conduct extensive experiments on multiple tasks in various domains, including regression, semantic segmentation, as well as natural language processing. The model architectures that we use include CNN, MLP and BERT. We perform 7 to 10 active learning cycles, and the annotation budget for each cycle ranges from 20 to more than 3000. All the reported results are averaged over 3 runs for a reliable evaluation, *unless specified otherwise*. All the data selections are carried without replacement, following the common practice in active learning literature. We conduct all the experiments using Pytorch [28] and our source code will be publicly available.

4.1 Image Classification

Setting. We adopt three benchmark classification datasets for evaluations, including MNIST [12], Cifar10 [13] and SVHN [14]. MNIST consists of 60000 training samples and we only use a small portion since it is an easy task. The experiments on MNIST are repeated 10 times and we report the averaged results. The Cifar10 dataset includes 50000 training and 10000 testing samples, uniformly distributed across 10 classes. SVHN includes 73257 training and 26032 testing samples, and we do not use the additional training data in SVHN, following the common practice. SVHN is a typical imbalanced dataset.

We use different architectures for these three tasks, including a small CNN for MNIST, VGG19 [29] for Cifar10 and ResNet-18 [30] for SVHN. The network and training details are described in Appendix A.3. Further, in Appendix A.4, we present additional results on Cifar10, Cifar100 and Caltech101 with ResNet-18 [30].

Observations. We compare our method with the state-of-the-art baselines and illustrate the results in Figure 1. The baseline methods include Random selection, Entropy, BALD [31, 32], QBC [33], CoreSet [19], VAAL [6], LL4AL [34], BADGE [22] and CoreGCN[‡] [7]. For the baseline algorithms, we use the hyper-parameters suggested in the original papers. For our method, we use the following hyper-parameters in all the experiments: $K = 30$ and $\zeta = 10^{-3}$, to ensure the constraint on noise magnitude.

As shown in Figure 1, our method (*NoiseStability*) outperforms or is comparable to the best baselines (in terms of accuracy) at all active learning cycles. In particular, our method usually yields a more rapid and stable increase of accuracy at the first several cycles, implying that noise stability is not

[‡]The released code reported an error when running on SVHN, so we evaluate SRAAL [35] instead.

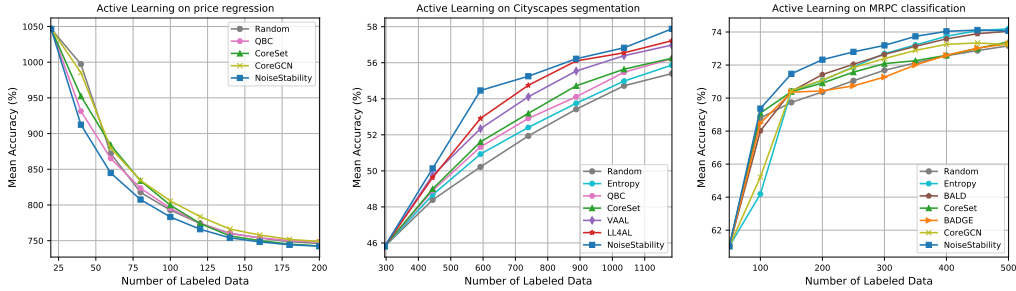


Figure 2: Active learning performance due to the different active learning methods on the regression task: Ames (**left**), semantic segmentation task: Cityscapes (**middle**), and natural language processing task: MRPC (**right**).

sensitive to the predictive accuracy and calibration. In addition, the superior results in the SVHN (and Caltech101 in Appendix) experiments demonstrate that our method is robust imbalanced datasets. We conjecture this is due to the simplicity of our method. In contrast, training auxiliary models [33, 6] with imbalanced data could be adverse to the auxiliary models themselves, thus leading to an inferior performance of the task model.

4.2 Other Tasks and Data Types

In this section, we validate our method with more diverse tasks, including regression, semantic segmentation and paraphrase recognition. For the regression task, we use data that includes both continuous and discrete variables, and we compare our method with the general algorithms that do not rely on probabilistic predictions. For the semantic segmentation task, we focus on the baselines that have been shown very effective for image data, e.g. LL4AL and VAAL. For the paraphrase recognition task, we use natural language data and make comparisons with the competitive baseline methods designed for classification problems, such as BALD and BADGE. General baselines Random and CoreSet are evaluated on all the three benchmarks. We present a brief result below, and refer readers to Appendix A.5 for detailed descriptions of the datasets and experimental configurations.

4.2.1 Regression Problem

We use the Ames Housing dataset [16] for this task. An MLP model takes a 215-dimensional feature as input and is trained to predict a real value as the house price. Compared with classification, the predictive output of regression does not explicitly contain information about uncertainty, which makes a part of active learning algorithms unavailable. The reported results are averaged over 50 runs for a reliable evaluation. As illustrated in Figure 2 (left), our method always yields the lowest mean absolute error before the performance saturation. We also observe that, the naive random selection becomes very competitive after the first two cycles, indicating that it is challenging for active learning to outperform passive learning in regression problems.

4.2.2 Semantic Segmentation

Semantic segmentation is more complex than image classification due to the requirement of high classification accuracy at pixel level. As a consequence, in several baseline methods, such as VAAL [6], the auxiliary models need a careful design in order to achieve a satisfactory performance. This increases the burden of deployment in real scenarios. In contrast, our method is free of extra design and can be easily adopted for this application, demonstrating its task-agnostic advantage. We illustrate the results in Figure 2 (middle), and observe a remarkable improvement of our method. Given the Cityscapes dataset is highly imbalanced, this experiment once again demonstrates the superiority of our method on imbalanced datasets.

4.2.3 Natural Language Processing

To further demonstrate the domain-agnostic nature of our method, we conduct an experiment on the Microsoft Research Paraphrase Corpus (MRPC) dataset, a classical NLP task aiming to identify whether two sentences are paraphrases of each other, by fine-tuning a pre-trained BERT model.

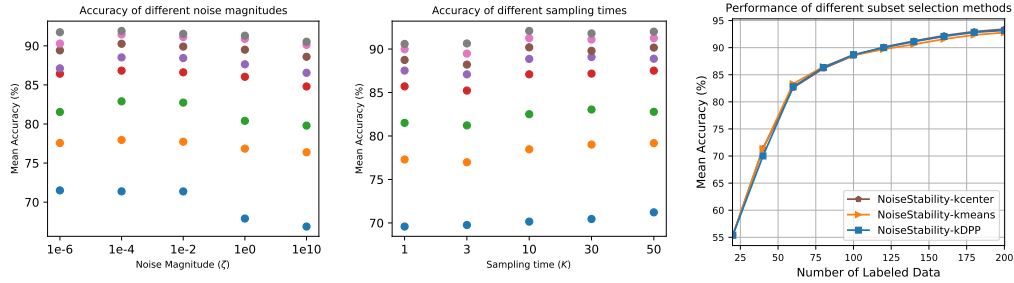


Figure 3: Evaluation of the different hyper-parameters on MNIST: noise magnitude λ (left), sampling times K (middle) and subset selection methods (right). In the left and middle plots, we use dots with different colors to denote different cycles, e.g. the blue dots at the bottom refer to cycle 2 and the grey dots at the top refer to cycle 9.

As shown in Figure 2 (right), our method exhibits significant superiority, demonstrating its wide applicability, whereas other state-of-the-art baselines perform less competitive in this task.

5 Discussion

In this section, we present further discussions on the efficacy of the proposed method. Firstly in Section 5.1, we study the choice of the hyper-parameters which are relevant to the noise sampling in our method. Then we conduct an ablation study to investigate the magnitude and direction of $\Delta z(\mathbf{x})$, respectively.

5.1 Sensitivity to Hyper-parameters (relevant to noise)

We firstly investigate how our algorithm is sensitive to the hyper-parameters (i.e. noise magnitude and sampling times). We conduct this set of experiments on MNIST.

Noise magnitude. An appropriate setting of the noise magnitude will benefit our method. Specifically, we observe that noise with a too large magnitude tends to destroy the learned knowledge in DNNs. We evaluate the choices of $\{10^{-6}, 10^{-4}, 10^{-2}, 1, 10\}$ respectively for the ζ . The results in Figure 3 (left) show that a ζ of between 10^{-4} and 10^{-2} is likely to yield good performance. A larger ζ leads to dramatic performance decrease at early cycles. Interestingly, we observe that a too small ζ also tends to be sub-optimal. We conjecture the reason may lie in that, if the noise is too trivial, only those activated neurons have output perturbations, making the final output deviation less informative.

Noise sampling times. Accurate approximations such as that for Eq (6) usually require considerable sampling times. However, we surprisingly find that our method is not that sensitive to the sampling times K . We study the choices of $\{1, 3, 10, 30, 50\}$ respectively for K . As shown in Figure 3 (middle), using $K = 10$ can deliver a very competitive performance. We conjecture this is because a random noise is sufficient to produce rich pattern perturbations for the parameters in DNNs, making the output deviation (due to only a few noise samplings) a reasonable criterion for unlabeled data selection (considering both magnitude and direction).

Subset selection. The topic of subset selection has been well studied in the machine learning community. Other classical algorithms can be easily integrated into our framework. We validate this by replacing our greedy k-center algorithm with kmeans++ [36] (suggested by BADGE) and k-DPP [37]. Figure 3 (right) shows that the three algorithms yield quite similar results in our framework.

5.2 Ablation Study

Here we demonstrate that both the gradient magnitude and direction are informative in subset selection. Specifically, we compare our method with its two degenerated versions including (1) *NoiseStability-M* which selects samples with maximum magnitude $\|\Delta z(\mathbf{x})\|_2$; and (2) *NoiseStability-D* which normalizes each $\Delta z(\mathbf{x})$ to unit magnitude before performing the greedy k-center selection.

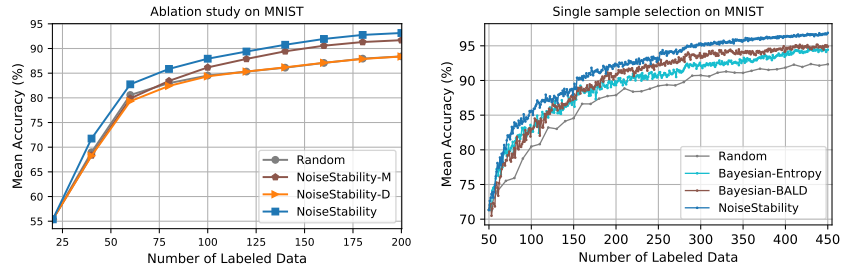


Figure 4: Comparison on MNIST with degenerated implementations (**left**) and with the Bayesian active learning methods with a selection size of 1 (**right**).

We observe in Figure 4 (left) that, neither of the two sub-optimal implementations can compete with the full version of our method.

We then investigate the effectiveness of the magnitude $\|\Delta z(\mathbf{x})\|_2$ on uncertainty estimation. This can be evaluated by the task of single sample selection, where diversity is no longer considered. We compare our method with the popular deep Bayesian active learning baselines on the MNIST dataset. For fair comparison, we perform 50 samplings for all the methods. As shown in Figure 4 (right), ours is superior to the baselines, demonstrating that noise stability is a reliable indicator of example uncertainty.

6 Related Work

Active learning has been a long-term open research topic in the community. Most of the methods can be categorized into three groups, namely uncertainty-based, diversity-based and synthesis-based. In this section, we provide an overview of the typical works.

Uncertainty-based. Traditional methods solve the problem mainly via estimating uncertainty for unlabeled data. Several typical works [38–43] have been proposed for shallow or statistical models. Nevertheless, as the rapid development of deep learning, a new challenge has emerged. That is, how to estimate data uncertainty with deep neural networks (DNNs). Several methods [6, 34, 35, 44] attempt to address this challenge with the aid of the highly customized DNNs and training fashions, such as VAE (variational auto-encoder) [45] and adversarial learning. [19, 33] explore combining a classical algorithm (e.g. K-center or 0-1 Knapsack problem) with DNNs to select the most uncertain data for annotation.

In context of deep learning, another category of methods resort to deep Bayesian inference, which approximates the uncertainty (e.g. measured by output entropy) over posterior probabilities. Our method lies in this category in nature. The most similar existing work to ours is MC-Dropout [4]. An essential difference lies in that, our method only requires a local noise sampling around a specific solution, whereas the Bayesian inference requires a global sampling over an entire hypothesis space. Our work is also relevant to the recent studies on linearized Laplace approximation of the BNN posterior [46, 47]. We refer readers to Appendix A.6 for a detailed discussion.

Diversity-based. This category of methods attempt to select unlabeled data that can diversify the labeled pool. The methods are also known as distribution-based [48–56]. Although the diversity-based methods were traditionally treated as essentially different from the uncertainty-based methods, it is worth noting that a recent study [57] argues that data diversity is correlated to data uncertainty.

Synthesis-based. This category of methods aim to diversify the labeled pool by synthesizing new diverse data that benefits the task model training. Typical methods [58, 59, 9] resort to generative models, such as GAN [60] or VAE [45], for data synthesis, creating an extra burden of training the auxiliary models.

7 Conclusion

We propose a simple yet robust method that leverages noise stability for uncertainty estimation in deep active learning. For an input sample, noise stability measures the stability of the output when

a random perturbation is imposed on the model parameters. The direction of the feature deviation is also utilized to ensure the diversity of selected examples. Our theoretical analyses prove that, the resulting deviation under a small parameter noise acts as a reasonable proxy of the gradient, in terms of both magnitude and direction. The extensive evaluations on multiple tasks demonstrate the superiority of the proposed method.

References

- [1] M. Gorriz, A. Carlier, E. Faure, and X. Giro-i Nieto, “Cost-effective active learning for melanoma segmentation,” *arXiv Preprint arXiv:1711.09168*, 2017.
- [2] K. Konyushkova, R. Sznitman, and P. Fua, “Learning active learning from data,” in *Proceedings of the Advances in Neural Information Processing Systems*, 2017, pp. 4225–4235.
- [3] P. Ren, Y. Xiao, X. Chang, P.-Y. Huang, Z. Li, B. B. Gupta, X. Chen, and X. Wang, “A survey of deep active learning,” *ACM Computing Surveys (CSUR)*, vol. 54, no. 9, pp. 1–40, 2021.
- [4] Y. Gal and Z. Ghahramani, “Dropout as a bayesian approximation: Representing model uncertainty in deep learning,” in *International Conference on Machine Learning*, 2016.
- [5] Y. Freund, H. S. Seung, E. Shamir, and N. Tishby, “Selective sampling using the query by committee algorithm,” *Machine Learning*, vol. 28, no. 2-3, pp. 133–168, 1997.
- [6] S. Sinha, S. Ebrahimi, and T. Darrell, “Variational adversarial active learning,” in *Proceedings of the IEEE International Conference on Computer Vision*, 2019, pp. 5972–5981.
- [7] R. Caramalau, B. Bhattarai, and T.-K. Kim, “Sequential graph convolutional network for active learning,” in *Proceedings of the IEEE/CVF Conference on Computer Vision and Pattern Recognition (CVPR)*, June 2021, pp. 9583–9592.
- [8] M. Ducoffe and F. Precioso, “Adversarial active learning for deep networks: a margin based approach,” *arXiv Preprint arXiv:1802.09841*, 2018.
- [9] C. Mayer and R. Timofte, “Adversarial sampling for active learning,” in *Proceedings of the IEEE Winter Conference on Applications of Computer Vision*, 2020, pp. 3071–3079.
- [10] C. M. Bishop, “Training with noise is equivalent to tikhonov regularization,” *Neural computation*, vol. 7, no. 1, pp. 108–116, 1995.
- [11] S. Arora, R. Ge, B. Neyshabur, and Y. Zhang, “Stronger generalization bounds for deep nets via a compression approach,” *ArXiv*, vol. abs/1802.05296, 2018.
- [12] Y. LeCun, L. Bottou, Y. Bengio, and P. Haffner, “Gradient-based learning applied to document recognition,” *Proceedings of the IEEE*, vol. 86, no. 11, pp. 2278–2324, 1998.
- [13] A. Krizhevsky, G. Hinton *et al.*, “Learning multiple layers of features from tiny images,” 2009.
- [14] Y. Netzer, T. Wang, A. Coates, A. Bissacco, B. Wu, and A. Y. Ng, “Reading digits in natural images with unsupervised feature learning,” in *NIPS Workshop on Deep Learning and Unsupervised Feature Learning*, 2011.
- [15] L. Fei-Fei, R. Fergus, and P. Perona, “One-shot learning of object categories,” *IEEE TPAMI*, vol. 28, no. 4, pp. 594–611, 2006.
- [16] D. De Cock, “Ames, iowa: Alternative to the boston housing data as an end of semester regression project,” *Journal of Statistics Education*, vol. 19, no. 3, 2011.
- [17] M. Cordts, M. Omran, S. Ramos, T. Rehfeld, M. Enzweiler, R. Benenson, U. Franke, S. Roth, and B. Schiele, “The cityscapes dataset for semantic urban scene understanding,” in *IEEE Conference on Computer Vision and Pattern Recognition*, 2016.
- [18] W. B. Dolan and C. Brockett, “Automatically constructing a corpus of sentential paraphrases,” in *Proceedings of the Third International Workshop on Paraphrasing (IWP2005)*, 2005.
- [19] O. Sener and S. Savarese, “Active learning for convolutional neural networks: A core-set approach,” in *International Conference on Learning Representations*, 2018.

- [20] A. Kirsch, J. Van Amersfoort, and Y. Gal, “Batchbald: Efficient and diverse batch acquisition for deep bayesian active learning,” *Advances in neural information processing systems*, vol. 32, pp. 7026–7037, 2019.
- [21] T. F. Gonzalez, “Clustering to minimize the maximum intercluster distance,” *Theoretical computer science*, vol. 38, pp. 293–306, 1985.
- [22] J. T. Ash, C. Zhang, A. Krishnamurthy, J. Langford, and A. Agarwal, “Deep batch active learning by diverse, uncertain gradient lower bounds,” in *International Conference on Learning Representations*, 2020.
- [23] C. Zhang, H. Kjellström, and S. Mandt, “Determinantal point processes for mini-batch diversification,” in *33rd Conference on Uncertainty in Artificial Intelligence, UAI 2017, Sydney, Australia, 11 August 2017 through 15 August 2017*. AUAI Press Corvallis, 2017.
- [24] B. Settles and M. Craven, “An analysis of active learning strategies for sequence labeling tasks,” in *proceedings of the 2008 conference on empirical methods in natural language processing*, 2008, pp. 1070–1079.
- [25] Y. Zhang, M. Lease, and B. Wallace, “Active discriminative text representation learning,” in *Proceedings of the AAAI Conference on Artificial Intelligence*, vol. 31, no. 1, 2017.
- [26] J. Huang, R. Child, V. Rao, H. Liu, S. Satheesh, and A. Coates, “Active learning for speech recognition: the power of gradients,” *arXiv preprint arXiv:1612.03226*, 2016.
- [27] B. Venkatesh and J. J. Thiagarajan, “Ask-n-learn: Active learning via reliable gradient representations for image classification,” *arXiv preprint arXiv:2009.14448*, 2020.
- [28] A. Paszke, S. Gross, S. Chintala, G. Chanan, E. Yang, Z. DeVito, Z. Lin, A. Desmaison, L. Antiga, and A. Lerer, “Automatic differentiation in pytorch,” 2017.
- [29] K. Simonyan and A. Zisserman, “Very deep convolutional networks for large-scale image recognition,” *arXiv Preprint arXiv:1409.1556*, 2014.
- [30] K. He, X. Zhang, S. Ren, and J. Sun, “Deep residual learning for image recognition,” in *Proceedings of the IEEE Conference on Computer Vision and Pattern Recognition*, 2016, pp. 770–778.
- [31] N. Houslyby, F. Huszár, Z. Ghahramani, and M. Lengyel, “Bayesian active learning for classification and preference learning,” *arXiv preprint arXiv:1112.5745*, 2011.
- [32] Y. Gal, R. Islam, and Z. Ghahramani, “Deep bayesian active learning with image data,” in *International Conference on Machine Learning*, 2017.
- [33] W. Kuo, C. Häne, E. Yuh, P. Mukherjee, and J. Malik, “Cost-sensitive active learning for intracranial hemorrhage detection,” in *International Conference on Medical Image Computing and Computer-Assisted Intervention*, 2018.
- [34] D. Yoo and I. S. Kweon, “Learning loss for active learning,” in *Proceedings of the IEEE Conference on Computer Vision and Pattern Recognition*, 2019, pp. 93–102.
- [35] B. Zhang, L. Li, S. Yang, S. Wang, Z.-J. Zha, and Q. Huang, “State-relabeling adversarial active learning,” in *Proceedings of the IEEE Conference on Computer Vision and Pattern Recognition*, 2020, pp. 8756–8765.
- [36] D. Arthur and S. Vassilvitskii, “k-means++: The advantages of careful seeding,” Stanford, Tech. Rep., 2006.
- [37] A. Kulesza and B. Taskar, “k-dpps: Fixed-size determinantal point processes,” in *ICML*, 2011.
- [38] A. J. Joshi, F. Porikli, and N. Papanikolopoulos, “Multi-class active learning for image classification,” in *Proceedings of the IEEE Conference on Computer Vision and Pattern Recognition*, 2009, pp. 2372–2379.
- [39] D. D. Lewis and J. Catlett, “Heterogeneous uncertainty sampling for supervised learning,” in *Machine learning proceedings*. Elsevier, 1994, pp. 148–156.
- [40] D. Roth and K. Small, “Margin-based active learning for structured output spaces,” in *Proceedings of the European Conference on Machine Learning*, 2006, pp. 413–424.
- [41] S. Tong and D. Koller, “Support vector machine active learning with applications to text classification,” *Journal of Machine Learning Research*, vol. 2, no. Nov, pp. 45–66, 2001.

- [42] S. Vijayanarasimhan and K. Grauman, “Large-scale live active learning: Training object detectors with crawled data and crowds,” *International Journal of Computer Vision*, vol. 108, no. 1-2, pp. 97–114, 2014.
- [43] X. Li and Y. Guo, “Multi-level adaptive active learning for scene classification,” in *Proceedings of the European Conference on Computer Vision*, 2014, pp. 234–249.
- [44] R. Mackowiak, P. Lenz, O. Ghorri, F. Diego, O. Lange, and C. Rother, “Cereals-cost-effective region-based active learning for semantic segmentation,” *arXiv Preprint arXiv:1810.09726*, 2018.
- [45] D. P. Kingma and M. Welling, “Auto-encoding variational bayes,” *arXiv Preprint arXiv:1312.6114*, 2013.
- [46] A. Immer, M. Bauer, V. Fortuin, G. Rätsch, and M. E. Khan, “Scalable marginal likelihood estimation for model selection in deep learning,” *arXiv preprint arXiv:2104.04975*, 2021.
- [47] E. Daxberger, E. Nalisnick, J. U. Allingham, J. Antorán, and J. M. Hernández-Lobato, “Bayesian deep learning via subnetwork inference,” in *International Conference on Machine Learning*. PMLR, 2021, pp. 2510–2521.
- [48] M. Bilgic and L. Getoor, “Link-based active learning,” in *NIPS Workshop on Analyzing Networks and Learning with Graphs*, 2009.
- [49] E. Elhamifar, G. Sapiro, A. Yang, and S. Shankar Sasrty, “A convex optimization framework for active learning,” in *Proceedings of the IEEE International Conference on Computer Vision*, 2013, pp. 209–216.
- [50] A. Freytag, E. Rodner, and J. Denzler, “Selecting influential examples: Active learning with expected model output changes,” in *Proceedings of the European Conference on Computer Vision*, 2014, pp. 562–577.
- [51] M. Hasan and A. K. Roy-Chowdhury, “Context aware active learning of activity recognition models,” in *Proceedings of the IEEE International Conference on Computer Vision*, 2015, pp. 4543–4551.
- [52] O. Mac Aodha, N. D. Campbell, J. Kautz, and G. J. Brostow, “Hierarchical subquery evaluation for active learning on a graph,” in *Proceedings of the IEEE Conference on Computer Vision and Pattern Recognition*, 2014, pp. 564–571.
- [53] H. T. Nguyen and A. Smeulders, “Active learning using pre-clustering,” in *International Conference on Machine Learning*, 2004.
- [54] N. Roy and A. McCallum, “Toward optimal active learning through monte carlo estimation of error reduction,” *International Conference on Machine Learning*, 2001.
- [55] Y. Yang, Z. Ma, F. Nie, X. Chang, and A. G. Hauptmann, “Multi-class active learning by uncertainty sampling with diversity maximization,” *International Journal of Computer Vision*, vol. 113, no. 2, pp. 113–127, 2015.
- [56] B. Settles, M. Craven, and S. Ray, “Multiple-instance active learning,” in *Proceedings of the Advances in Neural Information Processing Systems*, 2008, pp. 1289–1296.
- [57] A. Loquercio, M. Segu, and D. Scaramuzza, “A general framework for uncertainty estimation in deep learning,” *IEEE Robotics and Automation Letters*, vol. 5, no. 2, pp. 3153–3160, 2020.
- [58] J.-J. Zhu and J. Bento, “Generative adversarial active learning,” *arXiv Preprint arXiv:1702.07956*, 2017.
- [59] D. Mahapatra, B. Bozorgtabar, J.-P. Thiran, and M. Reyes, “Efficient active learning for image classification and segmentation using a sample selection and conditional generative adversarial network,” in *International Conference on Medical Image Computing and Computer-Assisted Intervention*, 2018.
- [60] I. Goodfellow, J. Pouget-Abadie, M. Mirza, B. Xu, D. Warde-Farley, S. Ozair, A. Courville, and Y. Bengio, “Generative adversarial nets,” in *Proceedings of the Advances in Neural Information Processing Systems*, 2014, pp. 2672–2680.
- [61] R. Vershynin, *High-dimensional probability: An introduction with applications in data science*. Cambridge university press, 2018, vol. 47.
- [62] D. P. Kingma and J. Ba, “Adam: A method for stochastic optimization,” *arXiv Preprint arXiv:1412.6980*, 2014.
- [63] L. Bottou, “Large-scale machine learning with stochastic gradient descent,” in *Proceedings of the COMP-STAT*. Springer, 2010, pp. 177–186.

- [64] N. Beck, D. Sivasubramanian, A. Dani, G. Ramakrishnan, and R. Iyer, “Effective evaluation of deep active learning on image classification tasks,” *arXiv preprint arXiv:2106.15324*, 2021.
- [65] A. Lang, C. Mayer, and R. Timofte, “Best practices in pool-based active learning for image classification,” 2021.
- [66] F. Yu, V. Koltun, and T. Funkhouser, “Dilated residual networks,” in *Proceedings of the IEEE Conference on Computer Vision and Pattern Recognition*, 2017, pp. 472–480.

A Appendix

A.1 Proof and Concentration of Eq (6)

A.1.1 Proof of Eq (6)

For brevity, we assume $f(\cdot; \theta)$ is a real-valued function parameterized by $\theta \in \mathbb{R}^n$, and the results can be naturally extended to a vector-valued function by aggregating the result w.r.t. each coordinate of the output vector.

Specifically, for each k , we firstly sample $\mathbf{t}^{(k)} \in \mathbb{R}^n$ from $\mathcal{N}(\mathbf{0}, \mathbf{I})$, and then get its direction $\mathbf{u}^{(k)}$ by self-normalization as $\mathbf{u}^{(k)} = \frac{\mathbf{t}^{(k)}}{\|\mathbf{t}^{(k)}\|_2}$. Since $\mathbf{u}^{(k)}$ is uniformly distributed over the unit sphere, the following equation is true:

$$\mathbb{E}[\mathbf{u}^{(k)} \mathbf{u}^{(k)T}] = \frac{1}{n} \mathbf{I}, \quad (10)$$

To avoid ambiguity, we use $\nabla_{\theta} f(\mathbf{x})$ to denote the gradient in all the following proofs, and omit the notation of the distribution under the expectation.

Proof. By applying Eq (10), we can expand the inner product between $\nabla_{\theta} f(\mathbf{x})$ and $\mathbf{u}^{(k)}$ in Eq (5) as

$$\begin{aligned} \mathbb{E}\|\widehat{\Delta}z(\mathbf{x})\|_2^2 &= \mathbb{E}\left\{\frac{n}{K} \sum_{k=1}^K \|\nabla_{\theta} f(\mathbf{x})^T \mathbf{u}^{(k)}\|_2^2\right\} \\ &= \frac{n}{K} \mathbb{E}\left\{\sum_{k=1}^K \nabla_{\theta} f(\mathbf{x})^T \mathbf{u}^{(k)} \mathbf{u}^{(k)T} f(\mathbf{x})\right\} \\ &= \frac{1}{K} \mathbb{E}\left\{\sum_{k=1}^K \nabla_{\theta} f(\mathbf{x})^T f(\mathbf{x})\right\} \\ &= \|\nabla_{\theta} f(\mathbf{x})\|_2^2. \end{aligned} \quad (11)$$

When $f(\cdot; \theta)$ is vector-valued, the above proof can be extended by applying Eq (11) to each dimension and then aggregate the result of each dimension by adding them together. We can do this for both sides of Eq (11), and the equation still holds. □

A.1.2 Concentration Inequality

We further present the concentration analysis of the empirical noise stability $\|\widehat{\Delta}z(\mathbf{x})\|_2^2$. The main result is:

Concentration of the gradient magnitude. *Let $\{\mathbf{u}^{(k)} \in \mathbb{R}^n | k = 1, 2, \dots, K\}$ be independent random directions, $\{\mathbf{x} | \mathbf{x} \in X_U\}$ be N unlabeled candidates, $\widehat{\Delta}z(\mathbf{x})$ be obtained by Eq (2) and $\nabla_{\theta} f(\mathbf{x}) \in \mathbb{R}^n$ be the gradient for a real-valued function f . We assume that $\epsilon > 0$, c and C are constants and $K \geq (C/\epsilon^2) \log N$. Then, with probability at least $1 - 2 \exp\{-c\epsilon^2 K\}$, we have*

$$\left| \|\widehat{\Delta}z(\mathbf{x})\|_2 - \|\nabla_{\theta} f(\mathbf{x})\|_2 \right| \leq \epsilon \|\nabla_{\theta} f(\mathbf{x})\|_2, \forall \mathbf{x} \in X_U. \quad (12)$$

Proof. To prove this, we construct a matrix $\mathbf{Q} \in \mathbb{R}^{K \times n}$ of which k -th row \mathbf{Q}_k is the transpose of $\sqrt{\frac{n}{K}} \mathbf{u}^{(k)}$. Then, by substituting the first order Taylor expansion, we have

$$\widehat{\Delta}z(\mathbf{x}) = \mathbf{Q} \nabla_{\theta} f(\mathbf{x}), \quad (13)$$

where \mathbf{Q} can be regarded as a scale-preserved random projection (in \mathbb{R}^n) onto a low-dimensional space \mathbb{R}^K . Then, the above concentration result can be proved by directly applying the Johnson-Lindenstrauss lemma (Theorem 5.3.1 in [61]). □

A.2 Proof and Concentration for Section 3.2

A.2.1 Proof of Eq (7) and Eq (8)

The proof of Eq (7) follows the same key idea of utilizing the property that the elements of the vector \mathbf{u} are uncorrelated, as shown in Eq (10). Using a proper scaling, \mathbf{Q} can be a scale-preserved random projection based on $\{\mathbf{u}^{(k)}\}_{k=1}^K$. Then, Eq (7) can be proved by

$$\mathbb{E}\|\widehat{\Delta z}(\mathbf{x}_i) - \widehat{\Delta z}(\mathbf{x}_j)\|_2^2 = \mathbb{E}\|\mathbf{Q}[\nabla_{\theta} f(\mathbf{x}_i) - \nabla_{\theta} f(\mathbf{x}_j)]\|_2^2 = \|\nabla_{\theta} f(\mathbf{x}_i) - \nabla_{\theta} f(\mathbf{x}_j)\|_2^2. \quad (14)$$

For proving Eq (8), we expand the quadratic terms on both sides of Eq (7) as

$$\begin{aligned} \mathbb{E}\|\widehat{\Delta z}(\mathbf{x}_i) - \widehat{\Delta z}(\mathbf{x}_j)\|_2^2 &= \mathbb{E}\|\widehat{\Delta z}(\mathbf{x}_i)\|_2^2 + \mathbb{E}\|\widehat{\Delta z}(\mathbf{x}_j)\|_2^2 - 2\mathbb{E}\langle \widehat{\Delta z}(\mathbf{x}_i), \widehat{\Delta z}(\mathbf{x}_j) \rangle, \\ \|\nabla_{\theta} f(\mathbf{x}_i) - \nabla_{\theta} f(\mathbf{x}_j)\|_2^2 &= \|\nabla_{\theta} f(\mathbf{x}_i)\|_2^2 + \|\nabla_{\theta} f(\mathbf{x}_j)\|_2^2 - 2\langle \nabla_{\theta} f(\mathbf{x}_i), \nabla_{\theta} f(\mathbf{x}_j) \rangle. \end{aligned} \quad (15)$$

Then substituting $\mathbb{E}\|\widehat{\Delta z}(\mathbf{x})\|_2^2$ with $\|\nabla_{\theta} f(\mathbf{x})\|_2^2$ (the known fact in Eq (6)) proves Eq (8).

A.2.2 Concentration Inequality

Concentration of the Euclidean distance. Let $\{\mathbf{u}^{(k)} \in \mathbb{R}^n | k = 1, 2, \dots, K\}$ be independent random directions, $\{\mathbf{x} | \mathbf{x} \in X_U\}$ be N unlabeled candidates, $\widehat{\Delta z}(\mathbf{x})$ be obtained by Eq (2) and $\nabla_{\theta} f(\mathbf{x}) \in \mathbb{R}^n$ be the gradient for a real-valued function f . We assume that $\epsilon > 0$, c and C are constants and $K \geq (C/\epsilon^2) \log N$. Then, with probability at least $1 - 2 \exp\{-c\epsilon^2 K\}$, we have

$$\left| \|\widehat{\Delta z}(\mathbf{x}_i) - \widehat{\Delta z}(\mathbf{x}_j)\|_2 - \|\nabla_{\theta} f(\mathbf{x}_i) - \nabla_{\theta} f(\mathbf{x}_j)\|_2 \right| \leq \epsilon \|\nabla_{\theta} f(\mathbf{x}_i) - \nabla_{\theta} f(\mathbf{x}_j)\|_2, \forall \mathbf{x}_i, \mathbf{x}_j \in X_U. \quad (16)$$

Note that both the formula and proof are the same as the concentration of the magnitude in Eq (12), as long as regarding $\nabla_{\theta} f(\mathbf{x}_i) - \nabla_{\theta} f(\mathbf{x}_j)$ as the original vector and \mathbf{Q} as the random projection.

Concentration of the inner product. When considering the inner product, we use normalized vectors to discuss the concentration property. This is because for pairwise similarity comparison, the angle between two vectors is more important to our analysis than the original inner product. Our main result is claimed as follows.

Let $\{\mathbf{u}^{(k)} \in \mathbb{R}^n | k = 1, 2, \dots, K\}$ be independent random directions, $\{\mathbf{x} | \mathbf{x} \in X_U\}$ be N unlabeled candidates, $\widehat{\Delta z}(\mathbf{x})$ be obtained by Eq (2), $\nabla_{\theta} f(\mathbf{x}) \in \mathbb{R}^n$ be the gradient for a real-valued function f and $g(\mathbf{x}) = \nabla_{\theta} f(\mathbf{x}) / \|\nabla_{\theta} f(\mathbf{x})\|_2$. We assume that $\epsilon > 0$, c and C are constants and $K \geq (C/\epsilon^2) \log N$. Then, with probability at least $1 - 2 \exp\{-c\epsilon^2 K\}$, we have

$$\frac{\langle g(\mathbf{x}_i), g(\mathbf{x}_j) \rangle - \epsilon}{(1 + \epsilon)^2} \leq \left\langle \frac{\widehat{\Delta z}(\mathbf{x}_i)}{\|\widehat{\Delta z}(\mathbf{x}_i)\|_2}, \frac{\widehat{\Delta z}(\mathbf{x}_j)}{\|\widehat{\Delta z}(\mathbf{x}_j)\|_2} \right\rangle \leq \frac{\langle g(\mathbf{x}_i), g(\mathbf{x}_j) \rangle + \epsilon}{(1 - \epsilon)^2}, \forall \mathbf{x}_i, \mathbf{x}_j \in X_U. \quad (17)$$

Proof. We further simplify $g(\mathbf{x}_i), g(\mathbf{x}_j)$ as $\mathbf{g}_i, \mathbf{g}_j$, respectively. Then by applying Eq (12) to $\mathbf{g}_i + \mathbf{g}_j$ and $\mathbf{g}_i - \mathbf{g}_j$, we have that with probability at least $1 - 2 \exp\{-c\epsilon^2 K\}$, the following two statements are true $\forall \mathbf{x}_i, \mathbf{x}_j \in X_U$:

$$\begin{aligned} (1 - \epsilon)\|\mathbf{g}_i + \mathbf{g}_j\|_2^2 &\leq \|\mathbf{Q}(\mathbf{g}_i + \mathbf{g}_j)\|_2^2 \leq (1 + \epsilon)\|\mathbf{g}_i + \mathbf{g}_j\|_2^2, \\ (1 - \epsilon)\|\mathbf{g}_i - \mathbf{g}_j\|_2^2 &\leq \|\mathbf{Q}(\mathbf{g}_i - \mathbf{g}_j)\|_2^2 \leq (1 + \epsilon)\|\mathbf{g}_i - \mathbf{g}_j\|_2^2. \end{aligned} \quad (18)$$

Then, we have that $\forall \mathbf{x}_i, \mathbf{x}_j \in X_U$, the following derivation is true with the same probability:

$$\begin{aligned}
\left\langle \frac{\widehat{\Delta z}(\mathbf{x}_i)}{\|\widehat{\Delta z}(\mathbf{x}_i)\|_2}, \frac{\widehat{\Delta z}(\mathbf{x}_j)}{\|\widehat{\Delta z}(\mathbf{x}_j)\|_2} \right\rangle &= \left\langle \frac{\mathbf{Q}\nabla_{\theta}f(\mathbf{x}_i)}{\|\mathbf{Q}\nabla_{\theta}f(\mathbf{x}_i)\|_2}, \frac{\mathbf{Q}\nabla_{\theta}f(\mathbf{x}_j)}{\|\mathbf{Q}\nabla_{\theta}f(\mathbf{x}_j)\|_2} \right\rangle \\
&= \frac{\mathbf{Q}\langle \nabla_{\theta}f(\mathbf{x}_i), \nabla_{\theta}f(\mathbf{x}_j) \rangle}{\|\mathbf{Q}\nabla_{\theta}f(\mathbf{x}_i)\|_2\|\mathbf{Q}\nabla_{\theta}f(\mathbf{x}_j)\|_2} \\
&\geq \frac{\mathbf{Q}\langle \nabla_{\theta}f(\mathbf{x}_i), \nabla_{\theta}f(\mathbf{x}_j) \rangle}{(1+\epsilon)^2\|\nabla_{\theta}f(\mathbf{x}_i)\|_2\|\nabla_{\theta}f(\mathbf{x}_j)\|_2} \\
&= \frac{\mathbf{Q}\langle \mathbf{g}_i, \mathbf{g}_j \rangle}{(1+\epsilon)^2} \\
&= \frac{1}{4(1+\epsilon)^2}(\|\mathbf{Q}(\mathbf{g}_i + \mathbf{g}_j)\|_2^2 - \|\mathbf{Q}(\mathbf{g}_i - \mathbf{g}_j)\|_2^2) \\
&\geq \frac{1}{4(1+\epsilon)^2}((1-\epsilon)\|\mathbf{g}_i + \mathbf{g}_j\|_2^2 - (1+\epsilon)\|\mathbf{g}_i - \mathbf{g}_j\|_2^2) \\
&= \frac{1}{4(1+\epsilon)^2}(4\langle \mathbf{g}_i, \mathbf{g}_j \rangle - 2\epsilon(\|\mathbf{g}_i\|_2^2 + \|\mathbf{g}_j\|_2^2)) \\
&= \frac{\langle \mathbf{g}_i, \mathbf{g}_j \rangle - \epsilon}{(1+\epsilon)^2}.
\end{aligned} \tag{19}$$

The other direction of Eq (17) can be similarly derived. Combining both directions completes the proof. \square

Remark. In all the three concentration guarantees, we involve the requirement of the noise sampling times K as $K \geq (C/\epsilon^2) \log N$, where N is the number of unlabeled candidates. The increment of K is only logarithmically proportional to the increment of N , indicating that noise stability is efficient in sampling. This partly explains why our algorithm is capable of achieving a decent performance with a relatively small K (e.g. $K = 10$).

A.3 Experiment Details for Image Classification

We use three different models for the selected benchmark datasets. The architectures and training details are described as follows.

MNIST. We use a small CNN with the architecture specified in Table 1. To train this task model, we use the Adam [62] optimizer with a learning rate of 1×10^{-3} and a batch size of 96. At each cycle, we train the model for 50 epochs with the labeled set.

Layer	# of Channels	Spatial Size
Input	1	28×28
Conv2d (1, 32, 5)	32	24×24
MaxPool2d	32	12×12
ReLU	32	12×12
Conv2d (32, 64, 5)	64	8×8
MaxPool2d	64	4×4
ReLU	64	4×4
Linear (1024, 128)	128	-
Linear (128, 10)	-	-

Table 1: The network architecture for MNIST classification.

Cifar10. For the Cifar10 task which is more challenging, we use VGG16 [29] as the task model. Specifically, we follow the practice in [7, 35] to adopt a special version[§] of VGG19 to make the model compatible with the lower image resolution (i.e. 32×32) in Cifar10. We use the SGD [63]

[§]<https://github.com/chengyangfu/pytorch-vgg-cifar10>

optimizer with a batch size of 128, a momentum of 0.9, a weight decay rate of 5×10^{-4} and an initial learning rate of 0.05. We train the model for 200 epochs and the learning rate is decayed by 0.5 every 30 epochs.

SVHN. We use ResNet-18 [30] as the task model for this experiment. Similar to the Cifar10 experiment, we adopt a special version[¶] to make the model compatible with the lower image resolution of 32×32 . At each cycle we use a batch size of 128 samples to train the task model with an initial learning rate of 0.1. The training continues for 200 epochs and we decay the learning rate by 0.1 at the 160th epoch. We employ the SGD [63] optimizer with a momentum of 0.9 and a weight decay rate of 5×10^{-4} .

A.4 Additional Experiments for Image Classification

We conduct extensive experiments using the ResNet-18 architecture, demonstrating the superiority of our algorithm for larger selection sizes (e.g. 2500) and higher image resolutions (e.g. 224×224).

Settings. We use Cifar10 [13], Cifar100 [13] and Caltech101 [15] for this group of experiments. The Cifar100 dataset includes 50000 training and 10000 testing samples, uniformly distributed across 100 classes. The Caltech101 dataset consists of 8677 images of higher resolution (e.g. 300×200 pixels), belonging to 101 categories. Caltech101 is a typical imbalanced dataset, where the number of the samples in a class varies from 40 to 800. For Cifar10 and Cifar100, we use the same settings as that for SVHN. For Caltech101, we use the original ResNet-18 and train the model for 50 epochs at each cycle. The initial learning rate is set to 0.01, decayed by 0.1 at the 40th epoch. Due to the higher image resolution, a smaller batch size of 64 is used to avoid GPU memory issues. We use a momentum of 0.9 and a weight decay rate of 5×10^{-4} with the SGD optimizer. For all the three datasets, during training we adopt standard data augmentations including random flip and crop.

Observations. We compare our algorithm with the baselines as mentioned in Section 4.1. Similarly, as shown in Figure 5, our algorithm exhibits notable superiority. Specifically, we observe that on standard balanced datasets Cifar10 and Cifar100, our NoiseStability is slightly leading the most competitive baselines, including Entropy, BADGE [22] and CoreGCN [7]. On Caltech101, our method yields remarkable improvements over the baselines.

Note that our observations are aligned with the conclusions in the recent studies [64, 65], which demonstrate that when data augmentation is used, advanced AL algorithms do not significantly outperform simple uncertainty-based methods (e.g. Entropy) on standard benchmarks. Nevertheless, advanced AL algorithms are more competitive on challenging datasets (e.g. imbalanced).

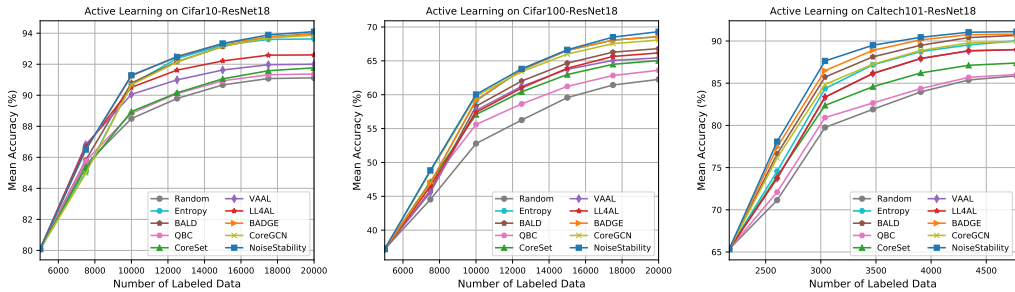


Figure 5: Classification performance due to the different active learning methods with ResNet-18 on Cifar10 (left), Cifar100 (middle) and Caltech101 (right).

A.5 Details of the Datasets Used in Section 4.2

A.5.1 Regression

Dataset. The Ames Housing dataset [16] describes the sales of individual residential properties in Ames, Iowa from 2006 to 2010. It includes 1461 labeled training samples and 60 explanatory

[¶]<https://github.com/kuangliu/pytorch-cifar>

attributes involved in assessing home values. This dataset is considered as an extended version of the classical Boston Housing dataset, which only has 506 labeled samples and 14 attributes.

Model and Training. We use 50% of the data for training and the remaining for testing. We follow common practices to transform the categorical features into numerical ones with one-hot encoding. A four-layer MLP is employed to extract features of the input vectors, and another fully connected layer is used as the predictor.

The Adam optimizer is adopted to train the task model. The training will continue for 500 epochs and the learning rate is set to 0.001. For our method, the output deviation w.r.t. a parameter noise is calculated on the final feature rather than the regression output.

A.5.2 Semantic Segmentation

Dataset. We use the Cityscapes [17], a large-scale street scene dataset. It includes images taken under various weather conditions in different seasons from 50 cities. Following widely used settings, we only use the standard training and validation data and crop the images to a dimension of 688×688 . There are 19 categories (classes) in total for each pixel, leading to a pixel-level classification problem. It is worth noting that the cropping size also depends on the task model.

Model and Training. Following a common practice [35], we choose a dilated residual network (DRN-D-22) [66] as the task model. It includes 8 layer modules and each module is composed of 1 or 2 *BasicBlock* of layers. One can refer to [66] for the network details .

Similar to the classification evaluations, we train the model for 7 cycles and 50 epochs for each cycle. Following the suggestion in [66], we use the Adam optimizer [62] with a learning rate of 5×10^{-4} , which remains unchanged during the entire training.

A.5.3 Natural Language Processing

Dataset. The Microsoft Research Paraphrase Corpus (MRPC) dataset [18] is a corpus of sentence pairs for recognizing whether the two sentences in each pair are semantically equivalent. It includes 3669 training samples and two thirds of them are positive. In general, this task can be treated as a binary classification one.

Model and Training. At each cycle, we fine-tune the standard BERT (bert-base-uncased) model for 10 epochs to ensure convergence. We follow the official guide of *Pytorch-Transformers-HuggingFace* to setup the other hyper-parameters. We use 50 initial labeled samples for training. At each cycle, 50 additional samples are selected for annotation.

A.6 Discussion of More Related Works

The studies in active learning with a linearized Laplace approximation of the BNN posterior [46, 47] are also relevant to our work. Here we briefly discuss their connections and differences. Theoretically, in terms of uncertainty (considering only the magnitude of the output deviation), our solution is the minimal mean-squared error estimation (MMSE) while theirs are Bayesian estimation, corresponding to the frequentist and Bayesian statistics, respectively. They are incompatible, yet inextricably linked. For instance, under the joint Gaussian conditions (such as the Gaussian priors assumed in those papers) the MAP and MMSE are known to be equivalent. They face similar computational challenges since MMSE is the conditional mean that is difficult to calculate as the MAP. Our approach is to approximate full conditional mean by the linear MMSE, which only pertains to the mean and covariances. This is a principled approach that is also used in practice in other areas such as the Kalman filter. In contrast, the Laplace approximation (e.g. Eq (3) in [46]) is accurate only when θ is close to the optimal value θ^* (where the first order term is negligible) and hence the theory only provides local guarantees. We argue that this condition is restrictive and not applicable to practical deep learning methods.